Nanoscale

PAPER

View Article Online
View Journal | View Issue

Cite this: *Nanoscale*, 2023, **15**, 3255

Anode-free Na metal batteries developed by nearly fully reversible Na plating on the Zn surface†

Olusola John Dahunsi, [a] Siyuan Gao,[a] Jacob Kaelin,[a] Bomin Li, [a] Iddrisu B. Abdul Razak, [b] Bowen An [a] and Yingwen Cheng *[a]

The anode-free battery architecture has recently emerged as a promising platform for lithium and sodium metal batteries as it not only offers the highest possible energy density, but also eliminates the need for handling hazardous metal electrodes during cell manufacturing. However, such batteries usually suffer from much faster capacity decay and are much more sensitive to even trace levels of irreversible side reactions on the anode, especially for the more reactive Na metal. This work systematically investigates electrochemical interfaces for Na plating and stripping and describes the use of the Zn surface to develop nearly fully reversible Na anodes with 1.0 M $NaPF_6$ in a diglyme-based electrolyte. The high performance includes consistently higher than 99.9% faradaic efficiencies for a wide range of cycling currents between 0.5 and 10 mA cm^{-2}, much more stable interfacial resistance and nearly no formation of mossy Na after 500 cycles compared with conventional Al and Cu surfaces. This improved reversibility was further confirmed under lean electrolyte conditions with a wide range of electrolyte concentrations and cycling temperatures and can be attributed to the strong interfacial binding and intrinsic sodiophilic properties of the Zn surface with Na, which not only ensured uniform Na plating but also eliminated most side reactions that would otherwise cause electrolyte depletion. As a result, full cells assembled with Na-free Zn foil and a high capacity $Na_3V_2(PO_4)_3$ cathode delivered ~90% capacity retention for 100 cycles, higher than the 73% retention of Cu foils and much higher than the 39% retention of Al foils. This work provides new approaches to enable stable cycling of anode-free batteries and contribute to their applications in practical devices.

Received 2nd November 2022,
Accepted 19th December 2022

DOI: 10.1039/d2nr06120a

rsc.li/nanoscale

Introduction

The need for stronger and more affordable batteries for electric transportation and smart grid applications is now widely recognized.[1] Current techno-economic analysis suggested that batteries with a specific energy density >400 W h kg^{-1} and cost <$100 W h per kg are needed to pave the road for successful deployments in practical large-scale applications, of which existing Li-ion electrochemistry is unlikely to be able to meet.[2–4] To this end, batteries designed with high capacity metal anodes with Earth-abundant elements, such as Na, K, Mg and Ca, are widely pursued as promising alternatives and among these, Na metal anodes are particularly attractive thanks to their abundancy, high capacity (1166 mA h g^{-1}), much lower cost and low redox potential of −2.714 V *vs.* the standard hydrogen electrode (SHE).[5–7] Unfortunately, similar to Li metal anodes, the cycling of Na metal also suffers from severe side reactions due to its aggressive chemical reactivity.[8,9] These side reactions spontaneously generate unstable solid–electrolyte interphases (SEI) that over time form thick and porous layers which disrupt Na-ion transport and cause the growth of unsafe dendrites, leading to premature cycling failure.[10–12]

Recently, substantial efforts have been devoted to enabling the stable and controllable cycling of Na metal anodes, and a plethora of advanced materials and electrolytes, such as artificial surface coating layers, novel electrolytes and additives, have been developed with promising results.[13–16] However, almost all these studies employ excess Na anodes (~400% or more) and flooded electrolytes (typically 50 μL) to account for irreversible anode and electrolyte consumption during cycling.[17–19] Such an excessive use of materials, although

[a]*Department of Chemistry and Biochemistry, Northern Illinois University, DeKalb, IL 60115, USA. E-mail: ycheng@niu.edu*
[b]*Department of Physics, Northern Illinois University, DeKalb, IL 60115, USA*

†Electronic supplementary information (ESI) available: Complete experimental details, ESI Tables S1–S3 including the estimated unit energy densities of SMB and Af-SMB in pouch and coin cell configurations, performance comparison of batteries developed in this work with typical half cells and anode-free batteries reported in the literature, ESI Fig. S1–S6: an equivalent circuit model for the analysis of the charge transfer resistance, SEM analysis of high capacity Na metal plating on Zn foil, voltage profile FEs as a function of electrolyte volume during the cycling of cells assembled using Zn and Cu foils, and XRD and TEM analyses of NVP powders. See DOI: https://doi.org/10.1039/d2nr06120a

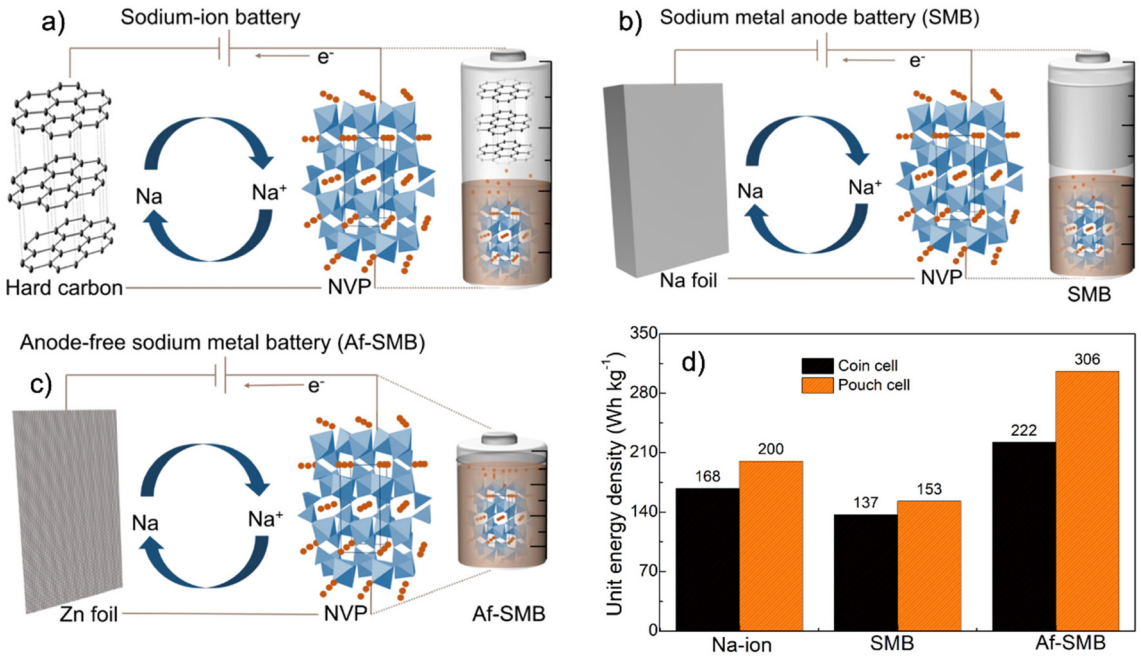

Fig. 1 Schematic illustrations of different cell designs for Na batteries using NVP as the cathode material: (a) Na-ion batteries using the hard carbon anode; (b) Na metal full cells with the initial presence of Na metal in excess amount; (c) anode-free full cells with Zn foil current collectors; (d) estimated unit energy densities of these three cell designs with experimental data.

ensuring outstanding cycling stability, significantly compromised the energy density of the cell to much lower than the theoretical value and only a fraction of that of Li-ion batteries (Fig. 1 and Tables S1 and S2†).[20–23] As such, unlocking the full potential of Na metal batteries requires practical strategies that support comparable stable cycling when ultrathin Na metal and a lean electrolyte are both employed, but has been very challenging as even a trace amount of side reactions would cause premature failure.[24–26] In principle, metallic Na is not required once a fully reversible Na metal anode architecture with 100% plating and stripping efficiency is utilized, as Na ions initially present in the cathode are sufficient to support continuous plating and stripping. This concept is known as the anode-free design and has attracted growing interest in recent years as it will not only provide the highest possible specific energy density, but also greatly simplify the cell manufacturing as safety regulations associated with metallic Na are no longer necessary (Fig. 1).

So far, previous works on anode-free batteries have mostly focused on Li metal batteries, but these works demonstrated the use of new electrolytes and surface modified current collectors, such as LiFSI-based concentrated electrolytes and functional modification layers composed of Al_2O_3 and polyacrylonitrile, for enabling >99% Li plating and stripping efficiency and eliminating the formation of problematic dendritic structures.[18,27] Recently, Cao *et al.* demonstrated that Na metal can be cycled with >99% efficiency on Cu foil using 4.0 M NaFSI in dimethoxyethane.[6] Similarly, high efficiencies were also obtained using 1.0 M $NaPF_6$ in diglyme on Cu foil and porous Al foils.[28,29] While these works showed impressive results, it is clear that they focus mostly on conventional current collectors without much effort on the systematic investigations of how current collector chemistry modulate the interfacial plating and stripping of Na, and as such, a fundamental understanding has not yet been established.[30,31]

This contribution aims at anode-free Na metal batteries and systematically evaluated several anode candidates and electrolyte combinations for enabling stable cycling of such batteries. Our results reveal the critical roles of the Zn surface

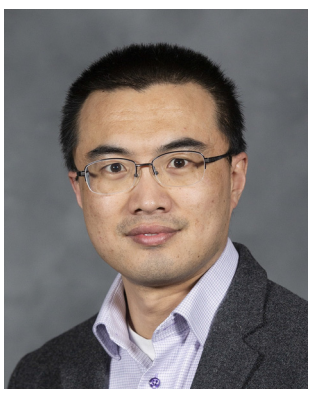

Yingwen Cheng

Dr Yingwen Cheng earned his B.S. degree in Chemistry and B.Eng. in Chemical Engineering from Shandong University in 2008 and Ph.D. in Chemistry from Duke University in 2013. He completed his postdoctoral training at Pacific Northwest National laboratory and joined Northern Illinois University in 2018. His group works on the problems associated with the chemistry of materials under electrochemical potential and aims to develop advanced materials and processes for the next-generation energy storage and conversion. He is a recipient of the 2021 Doctoral New Investigator Award from the Petroleum Research Fund of the American Chemical Society and is one of the 2023 Emerging Investigators from Nanoscale.

in directing nearly fully reversible Na plating and stripping, reaching faradaic efficiencies exceeding 99.90% with 1.0 M $NaPF_6$ in a glyme-based electrolyte that is much higher than the typical Cu and Al surfaces. Such a high efficiency was verified with a series of complimentary electroanalytical methods and was well retained in a wide range of current densities, electrolyte concentrations, volume and cycling temperature conditions. In addition, the plating of Na on the Zn surface exhibited almost zero nucleation overpotential compared with conventional Al and Cu surfaces and exhibited outstanding cycling stability for 500 cycles with negligible accumulation of dead mossy Na. Anode-free full cells assembled using a high-capacity $Na_3V_2(PO_4)_3$ cathode and Zn foils without the initial presence of Na metal delivered ~90% capacity retention for 100 cycles with high current cycling at 2.0 mA cm^{-2}. This work provides new insights into the anode–electrolyte surface chemistry to enable stable cycling of anode-free batteries and contribute to their applications in practical devices.

Results and discussion

We first evaluated the fundamental behavior of Na plating and stripping on Zn, Cu, and Al current collectors using cyclic voltammetry (CV) and a three-electrode setup inside an Ar-filled glovebox. The metal foil was used as the working electrode, and each has an exposed surface area of ~0.2 cm^{-2}. The electrolyte was 1.0 M $NaPF_6$ in diglyme and two pieces of Na ribbons were used as the reference and counter electrodes. Fig. 2a shows the comparison of the CV profiles acquired at 2 mV s^{-1} in the voltage window of −0.15–1.0 V and the tabulated key parameters. Overall, Na plating on the Zn surface exhibited an overpotential of only 13 mV, much lower than the 20 and 38 mV on Cu and Al surfaces, respectively. The corresponding Tafel analysis of these results reveals a much smaller slope of 6.0 mV dec^{-1} for Na plating on Zn compared with 11.0 mV dec^{-1} on Cu, correlating with enhanced Na plating kinetics (Fig. 2b). In addition, although amounts of Na plated on Zn and Cu were similar during testing, the anodic Na stripping peak was evidently stronger on Zn and this reveals a very high faradaic efficiency (FE) of 99.9%, also much higher than the 90.0% and 73.0% from Cu and Al foils, respectively.

The superior Na anode electrochemical performance on Zn foil is consistent with the affinity of Na metal on metal foils based on contact angle analysis.[32] Fig. 2c and d show the photographs of molten Na on Zn and Cu foils captured by placing and melting ~1 g Na metal on each foil inside a glove box at ~200 °C. Molten Na on Zn foil exhibited the smallest contact angle of ~32° and can be considered as sodiophilic, and this is in strong contrast with the sodiophobic properties of Cu where a much larger contact angle of ~115° was observed. The intrinsic sodiophilic properties of the Zn metal surface suggest that it can be used to direct uniform Na plating in batteries based on the plethora of literature demonstrations where direct correlations between contact angles and cycling stability were observed.[33–36] This was indeed confirmed with the ultra-flat surface morphology of 30 mA h cm^{-2} Na plated on Zn surfaces in scanning electron microscopy (SEM) and energy-dispersive X-ray spectroscopy (EDS) analysis (Fig. S1†).

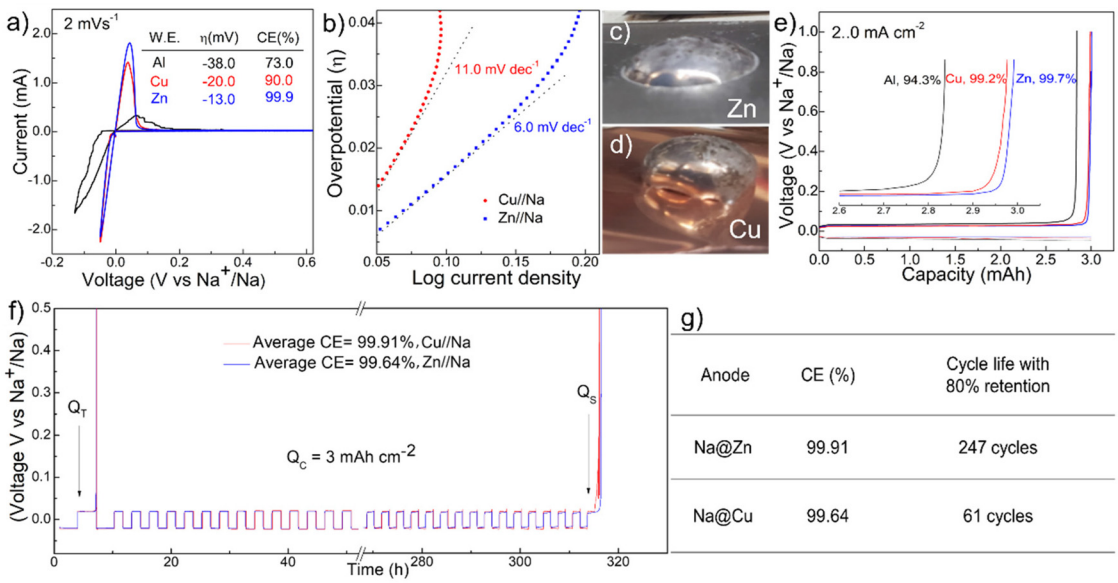

Fig. 2 Coulombic efficiency for Na plating and stripping on Zn, Cu and Al: (a) cyclic voltammograms and the tabulated key parameters for Na plating and stripping on Zn, Cu and Al foils; (b) Tafel plots from three-electrode testing; (c and d) photographs showing the contact angles of molten Na on Zn and Cu; (e) voltage profiles of half cells showing the plating–stripping efficiencies of Zn, Cu, and Al at 2.0 mA cm^{-2} and 3.0 mA h cm^{-2}; (f) voltage profiles showing the evaluated efficiencies of Zn and Cu after 100 cycles using a standard protocol; (g) cycle life projection of Zn and Cu half cells with the experimentally verified capacity.

We then assembled coin cells and evaluated Na plating/stripping behavior on these metal foils in a battery setup with 40 μL electrolyte. Fig. 2e shows the comparison of the voltage profiles at 2.0 mA cm^{-2} with a plating capacity of 3.0 mA h cm^{-2}. The FE quantified based on the ratio of stripping and plating capacities reveals a high efficiency of 99.7% when Zn foil was employed. This efficiency is clearly higher than the 99.2% and 94.3% of Cu and Al foils, respectively, and is consistent with the CV results. In addition, the high efficiency was further confirmed using the recently developed testing protocol for metal anodes that provide more reliable results.[37] In this protocol, the current collector was first conditioned by one cycle of plating and stripping 6.0 mA h cm^{-2} Na, followed by plating of 6.0 mA h cm^{-2} Na that functions as a Na reservoir (Q_T) for subsequent cycling. The cell was then cycled for 100 consecutive stripping and plating steps at 2.0 mA cm^{-2} with a capacity of 3.0 mA h cm^{-2} for each step. The electroactive Na remained after 100 cycles was quantified by complete stripping to 0.5 V and the quantified capacity was defined as the stripping capacity (Q_s). As such, the average FE can be determined using the following equation:[37]

$$FE_{avg} = \frac{nQ_c + Q_s}{nQ_c + Q_T} \quad (1)$$

where n is the number of cycles (100); Q_c = 3.0 mA h cm^{-2}; Q_T = 6.0 mA h cm^{-2}.

Fig. 2f presents the voltage profiles acquired on Zn and Cu current collectors using this protocol. Both batteries exhibited stable voltage profiles and similar overpotentials of ~75 mV at this high current density, but the remaining Na on Zn foils after cycling was more electrochemically active and delivered higher capacity. As a result, the average FE on Zn foil was 99.91%, higher than the 99.64% on Cu foil. The slightly higher FEs on Zn foils actually have strong impacts on the cycling stability, and in fact, our analysis suggests that an anode-free cell with this efficiency could last over 240 cycles for retaining 80% of the initial capacity whereas the Cu cell can only last for 61 cycles, confirming the outstanding potential of the new Zn–Na interface for practical batteries (Fig. 2g).

The outstanding performance of Zn foils in modulating Na plating and stripping was further confirmed in Zn//Na and Cu//Na coin cells at increasing current densities with the same plating capacity of 3.0 mA h cm^{-2} (Fig. 3a). The average FEs on the Zn current collector were all around 99.7% at 1.0, 3.0 and 5.0 mA cm^{-2} and decreased slightly to 96.1% at 10 mA cm^{-2}. The FEs for the cell assembled with Cu, in comparison, exhibited pronounced variations with increasing currents and decreased from 99.5% at 1.0 mA cm^{-2} to 96.5%, 92.5%, and 90.0% at 3.0, 5.0 and 10 mA cm^{-2}, respectively, suggesting more aggressive irreversible side-reactions on the Cu surface (Fig. 3b). Fig. 3c and d show the comparison of Nyquist plots acquired from Zn//Na and Cu//Na cells during cycling at 2.0 mA cm^{-2} and 3.0 mA h cm^{-2}. The analysis of these plots using the equivalent circuit model in Fig. S2† suggests the charge-transfer resistances (R_{ct}) for the Zn//Na cell increased from the initial 5.5 to 27.1 Ω cm^{-2} after 200 cycles, which is substantially smaller than the 12.2 to 225.1 Ω cm^{-2} increase for the Cu//Na cell. In addition, Fig. 3e and f show the compared photographs and SEM images of Zn and Cu foils after 200 cycles in the fully stripped state. The Zn foil remained shiny with nearly no residue tarnishing Na layers (commonly described as dead mossy Na) whereas the presence of such layers was evident on Cu foils. This mossy Na appeared as islands on Cu foil as a result of its highly sodiophobic properties as presented above due to the island type hetero-

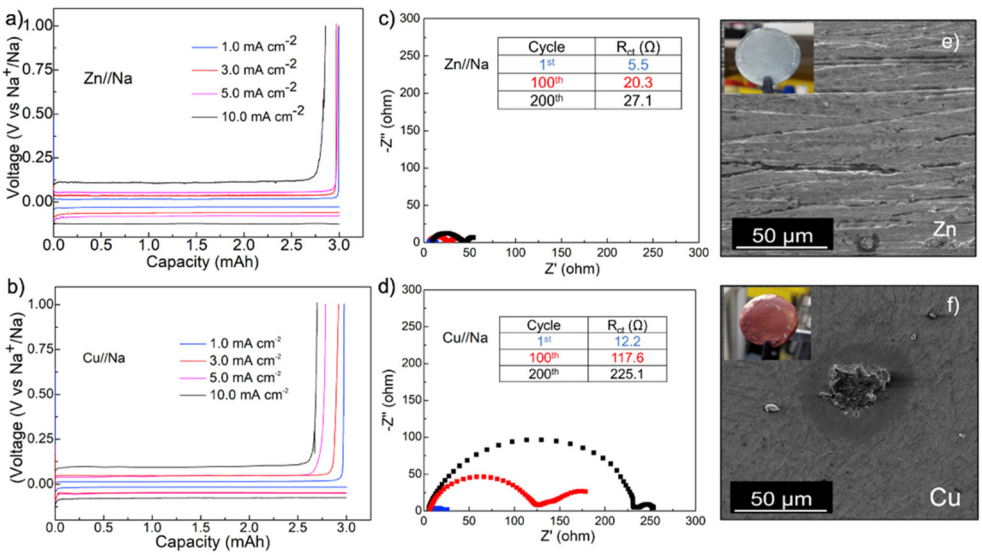

Fig. 3 Rate and cycling stability of Na plating and stripping in coin cells: voltage profiles at increasing current densities on (a) Zn and (b) Cu foils; Nyquist plots of (c) Zn//Na and (d) Cu//Na cells after 1, 100, and 200 cycles at 2.0 mA cm^{-2}; SEM images and photographs (inset) of (e) Zn and (f) Cu foils after 200 cycles.

geneous nucleation and growth.[38–41] Further EDS elemental analysis of the SEI layers on Zn reveals Na and F as the main components with overlapping elemental distribution (Fig. S3†), which is consistent with the observation of NaF diffraction peaks in the cycled Zn electrode and suggests that inorganic NaF is the main component in the SEI (Fig. S4†). Other than NaF, the cycled Zn electrodes only show diffraction peaks from Zn and the possible formation of NaZn alloys during cycling was excluded. Of note is that the formation of NaF-rich SEI layers promotes a uniform Na^+ flux and nondendritic Na growth and is presumably the reason behind the much more stable R_{ct} during cycling.[28]

We further performed battery testing under lean electrolyte conditions to better quantify the efficiency of Na^+/Na redox processes and demonstrate the practical applications of Zn foils in enabling high energy density batteries. Fig. 4a shows the comparison of dynamics of FEs during cycling as a function of electrolyte volume on Zn and Cu foils at 2.0 mA cm^{-2} with a plating capacity of 3.0 mA h cm^{-2} (Fig. S5 and 6†). The cycling with 20 μL electrolyte exhibited results that are similar to flooded conditions for the Zn//Na cell with very stable FEs higher than 99.9% for the entire 500 cycles. The FEs for the Cu//Na cell, although are fairly stable for the initial 200 cycles, exhibited pronounced fluctuations after 200 cycles (Fig. 4a). The high and stable FEs on Zn foils were well maintained when the electrolyte volume was reduced to 10 and 5 μL as shown in Fig. 4b. Cycling with 5 μL electrolyte, in particular, can still deliver >99.9% for more than 150 cycles and provides strong evidence on the crucial roles of the Zn surface in enabling fully reversible Na plating–stripping over long cycles with nearly no electrolyte depletion.

The outstanding performance of Zn foils for Na metal anodes appears depending strongly on the electrolyte composition, as can be seen in Fig. 4c and d with voltage profiles as a function of $NaPF_6$ concentration (0.5, 1.0 and 2.0 M in diglyme). These cells exhibited the expected concentration-dependent polarization with the smallest polarization for the most conductive 2.0 M electrolyte, 1.0 M $NaPF_6$ exhibited the best efficiency of 99.2% and this is slightly higher than the 97.4% and 95.5% from 2.0 M and 0.5 M electrolytes, respectively. Reasons behind such a pronounced concentration-dependent efficiency are unclear at this time but are consistent with prior observations.[22,23,28] In comparison, we further evaluated the efficiencies of other Na electrolytes and observed that they were unable to achieve such high reversibility as 1.0 M $NaPF_6$ in diglyme. In addition, although it is generally observed that batteries degrade faster at elevated temperatures due to the increased reactivity of side reactions,[42,43] Na plating on Zn foil exhibited an efficiency of 99.3% at 50 °C, which is nearly identical compared with 99.2% at 25 °C, thus confirming the outstanding interfacial stability and minimal side-reactions with 1.0 M $NaPF_6$ in a diglyme-based electrolyte. This electrolyte formulation appears essential for the outstanding stability, as the same analysis with other typical electrolytes, including 1.0 M $NaPF_6$ in carbonates, all exhibited significantly lower efficiencies (Fig. S7†).

We then evaluated the application of the Zn surface toward anode-free Na metal batteries using the high energy density

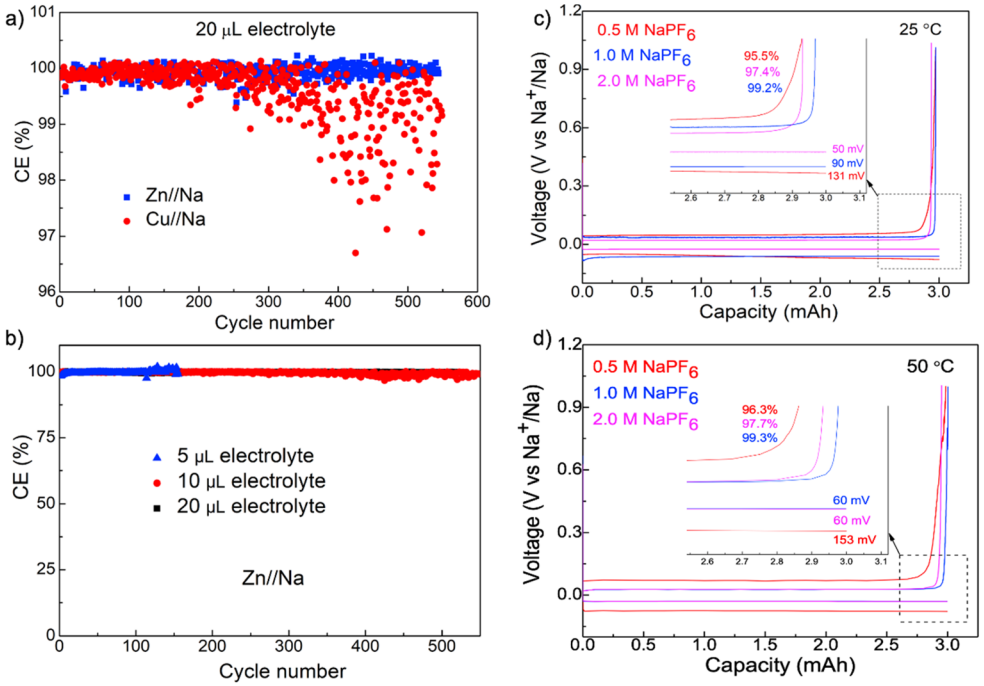

Fig. 4 Stability of Na plating and stripping on the Zn surface as a function of electrolyte volume, concentration and temperature: (a) faradaic efficiency of Zn//Na and Cu//Na cells using 20 μL of electrolyte; (b) efficiency of Zn//Na using gradually lowered electrolyte volumes; voltage profiles of the Zn//Na cell evaluated at (c) 25 and (d) 50 °C with 0.5, 1.0 and 2.0 M $NaPF_6$. All cells were cycled at 2.0 mA cm^{-2} and 3.0 mA h cm^{-2}.

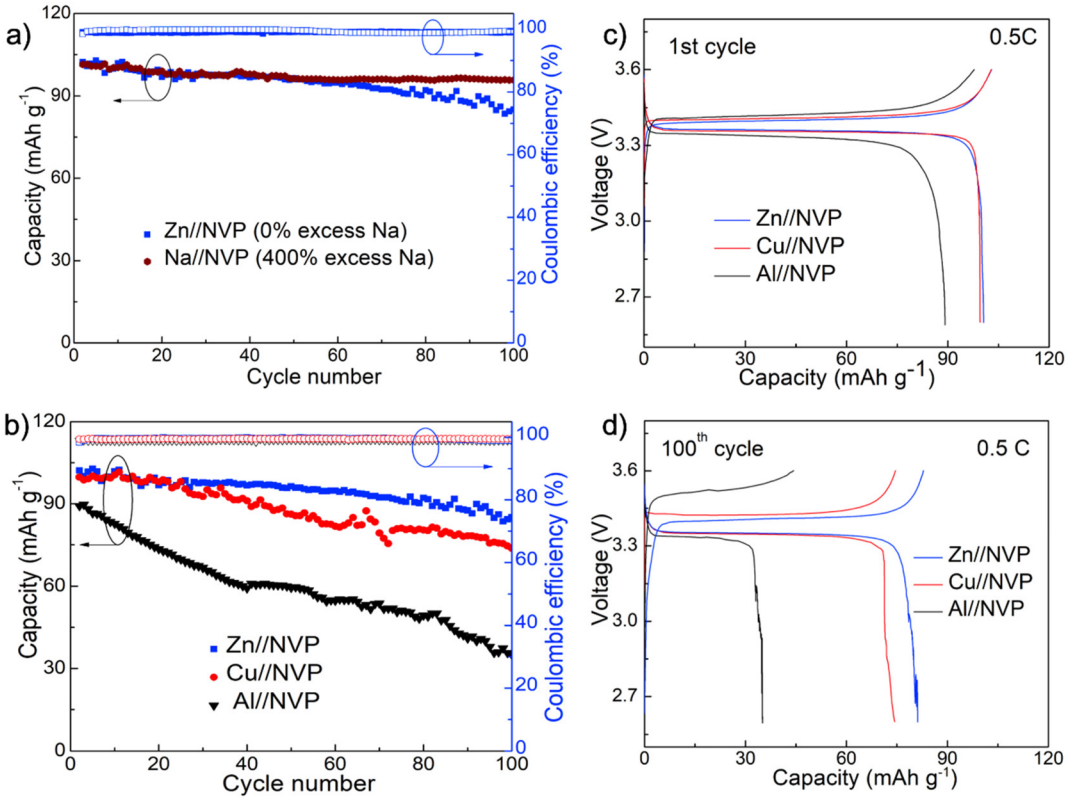

Fig. 5 Electrochemical performance of anode-free Na metal full batteries: (a) capacity retention and CE of Zn//NVP and Na//NVP full cells; (b) capacity retention and CE of Zn//NVP, Cu//NVP, and Al//NVP anode-free cells; (c and d) charge/discharge voltage profiles of Zn//NVP, Cu//NVP, and Al//NVP anode-free cells for the 1st and 100th cycles.

and cycling stable $Na_3V_2(PO4)_3$ (NVP) as the cathode material. This cathode was synthesized as composites with carbon nanotubes using a typical hydrothermal method as described in our previous work.[44] The phase purity and morphology of the as-synthesized powders were verified using X-ray diffraction and transmission electron microscopy (TEM) analyses prior to battery assembly and testing (Fig. S8 and S9†). As a standard comparison, we first compared the cycling stability of the anode-free Na full cell equipped with Zn foil with a regular Na metal battery containing ~400% excess Na. These two batteries were assembled using the same amount of the cathode and electrolyte and were cycled at 0.5C (1C = 118 mA h g^{-1}). The comparison of capacity retention and voltage profiles during cycling reveals that the anode-free Zn//NVP cell delivered a comparable capacity to the standard Na//NVP cell for the first 50 cycles and overall exhibited 87% capacity retention for 100 cycles, which is only slightly smaller than 93% of the standard cell (Fig. 5a).

The superior performance of Zn surfaces for anode-free batteries was clearly demonstrated when compared with the conventional Cu and Al foils. Specifically, Fig. 5b–d show the comparison of the cycling stability and the associated voltage profiles for the three anode-free batteries assembled with different metal foil current collectors. Although the Cu-based cell exhibited a similar initial capacity and voltage profile to the Zn cell for the first 20 cycles, the cell experienced much faster capacity decay to ~70% after 100 cycles along with increased overpotentials. The Al-based anode-free batteries, on the other hand, delivered a lower specific capacity and capacity retention due to the unstable anode–electrolyte interface. Nevertheless, the results confirm the importance of Zn in directing nearly fully reversible Na anodes, and we expect that further material development such as *via* structured hosts and/or carefully engineered Zn nucleation sites could further enhance the overall cell performance and be deployed as practical Na metal-free high energy density batteries.

Conclusions

Anode-free metal batteries are attractive in many aspects but are seriously constraint with rapid capacity fading. This study systematically examined several candidate electrode and electrolyte combinations using a relatively well-defined system and identified the Zn surface as capable of providing nearly fully reversible Na plating and stripping. Faradic efficiencies consistently higher than 99.90% were observed in a wide range of extreme reaction conditions including high current, lean electrolyte, and high temperatures, thus clearly verifying the intrinsic stability of the interface compared with the widely

employed Cu and Al surfaces. Such stability also enabled superior stability, with nearly unchanged >99.9% efficiency during 500 extreme capacity cycling at 3.0 mA h cm^{-2} and negligible formation of dead mossy Na on the Zn surface. As a result, Na-metal free full cells coupled with Zn foil and high capacity NVP cathodes without the initial presence of Na metal delivered ~90% capacity retention for 100 cycles, much better than the conventional Cu and Al foils. As such, our work confirms the potential of anode-free Na metal batteries and further anode architecture design based on a better balanced Zn surface could enable further enhanced cyclic stability for practical application.

Conflicts of interest

There are no conflicts to declare.

Acknowledgements

We greatly appreciate the insightful suggestions from Dr Christopher Johnson of Argonne National laboratory. This work was supported by the startup funds from Northern Illinois University. The use of the Center for Nanoscale Materials, an Office of Science user facility, was supported by the US Department of Energy, Office of Science, Office of Basic Energy Sciences, under contract no. DE-AC02-06CH11357.

References

1 D. M. Davies, M. G. Verde, O. Mnyshenko, Y. R. Chen, R. Rajeev, Y. S. Meng and G. Elliott, *Nat. Energy*, 2019, **4**, 42–50.
2 A. Kasliwal, N. J. Furbush, J. H. Gawron, J. R. McBride, T. J. Wallington, R. D. De Kleine, H. C. Kim and G. A. Keoleian, *Nat. Commun.*, 2019, **10**, 1555.
3 A. J. Louli, A. Eldesoky, R. Weber, M. Genovese, M. Coon, J. deGooyer, Z. Deng, R. T. White, J. Lee, T. Rodgers, R. Petibon, S. Hy, S. J. H. Cheng and J. R. Dahn, *Nat. Energy*, 2020, **5**, 693–702.
4 P. Albertus, S. Babinec, S. Litzelman and A. Newman, *Nat. Energy*, 2018, **3**, 16–21.
5 W. Luo, J. Wan, B. Ozdemir, W. Bao, Y. Chen, J. Dai, H. Lin, Y. Xu, F. Gu, V. Barone and L. Hu, *Nano Lett.*, 2015, **15**, 7671–7677.
6 R. Cao, K. Mishra, X. Li, J. Qian, M. H. Engelhard, M. E. Bowden, K. S. Han, K. T. Mueller, W. A. Henderson and J.-G. Zhang, *Nano Energy*, 2016, **30**, 825–830.
7 B. Lee, E. Paek, D. Mitlin and S. W. Lee, *Chem. Rev.*, 2019, **119**, 5416–5460.
8 J.-Y. Hwang, S.-T. Myung and Y.-K. Sun, *Chem. Soc. Rev.*, 2017, **46**, 3529–3614.
9 Z. Xu, J. Yang, T. Zhang, L. Sun, Y. Nuli, J. Wang and S.-i. Hirano, *Adv. Funct. Mater.*, 2019, **29**, 1901924.
10 S. Choudhury, S. Wei, Y. Ozhabes, D. Gunceler, M. J. Zachman, Z. Tu, J. H. Shin, P. Nath, A. Agrawal, L. F. Kourkoutis, T. A. Arias and L. A. Archer, *Nat. Commun.*, 2017, **8**, 898.
11 B. Sun, P. Li, J. Zhang, D. Wang, P. Munroe, C. Wang, P. H. L. Notten and G. Wang, *Adv. Mater.*, 2018, **30**, 1801334.
12 S. Wei, S. Xu, A. Agrawral, S. Choudhury, Y. Lu, Z. Tu, L. Ma and L. A. Archer, *Nat. Commun.*, 2016, **7**, 1–10.
13 J. Qin, H. Shi, K. Huang, P. Lu, P. Wen, F. Xing, B. Yang, M. Ye, Y. Yu and Z.-S. Wu, *Nat. Commun.*, 2021, **12**, 5786.
14 L. Wang, J. Shang, Q. Huang, H. Hu, Y. Zhang, C. Xie, Y. Luo, Y. Gao, H. Wang and Z. Zheng, *Adv. Mater.*, 2021, **33**, 2102802.
15 X. Zheng, Z. Gu, J. Fu, H. Wang, X. Ye, L. Huang, X. Liu, X. Wu, W. Luo and Y. Huang, *Energy Environ. Sci.*, 2021, **14**, 4936–4947.
16 S. Choudhury, S. Wei, Y. Ozhabes, D. Gunceler, M. J. Zachman, Z. Tu, J. H. Shin, P. Nath, A. Agrawal and L. F. Kourkoutis, *Nat. Commun.*, 2017, **8**, 1–10.
17 S. Park, H.-J. Jin and Y. S. Yun, *ACS Sustainable Chem. Eng.*, 2020, **8**, 17697–17706.
18 J. Qian, B. D. Adams, J. Zheng, W. Xu, W. A. Henderson, J. Wang, M. E. Bowden, S. Xu, J. Hu and J.-G. Zhang, *Adv. Funct. Mater.*, 2016, **26**, 7094–7102.
19 S. Chen, C. Niu, H. Lee, Q. Li, L. Yu, W. Xu, J.-G. Zhang, E. J. Dufek, M. S. Whittingham and S. Meng, *Joule*, 2019, **3**, 1094–1105.
20 R. Usiskin, Y. Lu, J. Popovic, M. Law, P. Balaya, Y.-S. Hu and J. Maier, *Nat. Rev. Mater.*, 2021, **6**, 1020–1035.
21 Y. Li, Q. Zhou, S. Weng, F. Ding, X. Qi, J. Lu, Y. Li, X. Zhang, X. Rong, Y. Lu, X. Wang, R. Xiao, H. Li, X. Huang, L. Chen and Y.-S. Hu, *Nat. Energy*, 2022, **7**, 511–519.
22 Y.-M. Lin, H.-S. Fan, C.-Z. Zhu and J. Xu, *Rare Met.*, 2022, **41**, 4104–4115.
23 D.-L. Ba, W.-H. Zhu, Y.-Y. Li and J.-P. Liu, *Rare Met.*, 2022, **41**, 4075–4085.
24 J. Liu, Z. Bao, Y. Cui, E. J. Dufek, J. B. Goodenough, P. Khalifah, Q. Li, B. Y. Liaw, P. Liu, A. Manthiram, Y. S. Meng, V. R. Subramanian, M. F. Toney, V. V. Viswanathan, M. S. Whittingham, J. Xiao, W. Xu, J. Yang, X.-Q. Yang and J.-G. Zhang, *Nat. Energy*, 2019, **4**, 180–186.
25 H. Chen, Y. Yang, D. T. Boyle, Y. K. Jeong, R. Xu, L. S. de Vasconcelos, Z. Huang, H. Wang, H. Wang, W. Huang, H. Li, J. Wang, H. Gu, R. Matsumoto, K. Motohashi, Y. Nakayama, K. Zhao and Y. Cui, *Nat. Energy*, 2021, **6**, 790–798.
26 X. Zheng, L. Huang, X. Ye, J. Zhang, F. Min, W. Luo and Y. Huang, *Chem*, 2021, **7**, 2312–2346.
27 N. A. Sahalie, Z. T. Wondimkun, W.-N. Su, M. A. Weret, F. W. Fenta, G. B. Berhe, C.-J. Huang, Y.-C. Hsu and B. J. Hwang, *ACS Appl. Energy Mater.*, 2020, **3**, 7666–7679.
28 Z. W. Seh, J. Sun, Y. Sun and Y. Cui, *ACS Cent. Sci.*, 2015, **1**, 449–455.
29 S. Liu, S. Tang, X. Zhang, A. Wang, Q.-H. Yang and J. Luo, *Nano Lett.*, 2017, **17**, 5862–5868.

30 B. Ma, Y. Lee and P. Bai, *Adv. Sci.*, 2021, **8**, 2005006.
31 A. P. Cohn, N. Muralidharan, R. Carter, K. Share and C. L. Pint, *Nano Lett.*, 2017, **17**, 1296–1301.
32 S. Tang, Y.-Y. Zhang, X.-G. Zhang, J.-T. Li, X.-Y. Wang, J.-W. Yan, D.-Y. Wu, M.-S. Zheng, Q.-F. Dong and B.-W. Mao, *Adv. Mater.*, 2019, **31**, 1807495.
33 M. Ohring, *Materials science of thin films: deposition & structure*, Elsevier, 2001.
34 P. Hartmann, T. Leichtweiss, M. R. Busche, M. Schneider, M. Reich, J. Sann, P. Adelhelm and J. Janek, *J. Phys. Chem. C*, 2013, **117**, 21064–21074.
35 H.-J. Chang, X. Lu, J. F. Bonnett, N. L. Canfield, K. Han, M. H. Engelhard, K. Jung, V. L. Sprenkle and G. Li, *J. Mater. Chem. A*, 2018, **6**, 19703–19711.
36 D. Jin, S. Choi, W. Jang, A. Soon, J. Kim, H. Moon, W. Lee, Y. Lee, S. Son, Y.-C. Park, H. Chang, G. Li, K. Jung and W. Shim, *ACS Appl. Mater. Interfaces*, 2019, **11**, 2917–2924.
37 B. D. Adams, J. Zheng, X. Ren, W. Xu and J.-G. Zhang, *Adv. Energy Mater.*, 2018, **8**, 1702097.
38 Z. Hou, Y. Yu, W. Wang, X. Zhao, Q. Di, Q. Chen, W. Chen, Y. Liu and Z. Quan, *ACS Appl. Mater. Interfaces*, 2019, **11**, 8148–8154.
39 C. Zhang, W. Lv, G. Zhou, Z. Huang, Y. Zhang, R. Lyu, H. Wu, Q. Yun, F. Kang and Q.-H. Yang, *Adv. Energy Mater.*, 2018, **8**, 1703404.
40 J. Luan, Q. Zhang, H. Yuan, D. Sun, Z. Peng, Y. Tang, X. Ji and H. Wang, *Adv. Sci.*, 2019, **6**, 1901433.
41 Z. Sun, H. Jin, Y. Ye, H. Xie, W. Jia, S. Jin and H. Ji, *ACS Appl. Energy Mater.*, 2021, **4**, 2724–2731.
42 H.-G. Jung, M. W. Jang, J. Hassoun, Y.-K. Sun and B. Scrosati, *Nat. Commun.*, 2011, **2**, 516.
43 J. Shim, R. Kostecki, T. Richardson, X. Song and K. A. Striebel, *J. Power Sources*, 2002, **112**, 222–230.
44 O. J. Dahunsi, B. Li, S. Gao, K. Lu, F. Xia, T. Xu and Y. Cheng, *ACS Appl. Energy Mater.*, 2022, **5**, 20–26.